

Simulated impacts of afforestation in East China monsoon region as modulated by ocean variability

**Di Ma, Michael Notaro, Zhengyu Liu,
Guangshan Chen & Yongqiang Liu**

Climate Dynamics

Observational, Theoretical and
Computational Research on the Climate
System

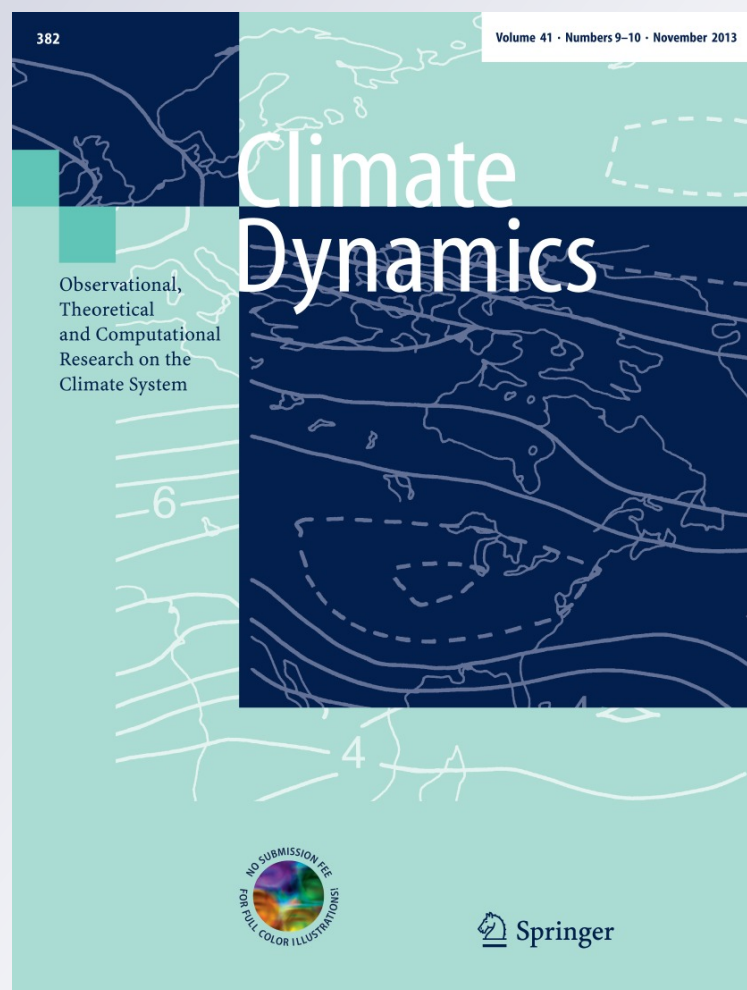
ISSN 0930-7575

Volume 41

Combined 9-10

Clim Dyn (2013) 41:2439-2450

DOI 10.1007/s00382-012-1592-9



Your article is protected by copyright and all rights are held exclusively by Springer-Verlag Berlin Heidelberg. This e-offprint is for personal use only and shall not be self-archived in electronic repositories. If you wish to self-archive your article, please use the accepted manuscript version for posting on your own website. You may further deposit the accepted manuscript version in any repository, provided it is only made publicly available 12 months after official publication or later and provided acknowledgement is given to the original source of publication and a link is inserted to the published article on Springer's website. The link must be accompanied by the following text: "The final publication is available at link.springer.com".

Simulated impacts of afforestation in East China monsoon region as modulated by ocean variability

Di Ma · Michael Notaro · Zhengyu Liu ·
Guangshan Chen · Yongqiang Liu

Received: 17 July 2012 / Accepted: 5 November 2012 / Published online: 21 November 2012
© Springer-Verlag Berlin Heidelberg 2012

Abstract Using the National Center for Atmospheric Research Community Climate System Model Version 3.5, this paper examines the climatic effects of afforestation in the East China monsoon region with a focus on land–atmosphere interactions and the modulating influence of ocean variability. In response to afforestation, the local surface air temperature significantly decreases in summer and increases in winter. The summer cooling is attributed to enhanced evapotranspiration from increased tree cover. During winter, afforestation induces greater roughness and weaker winds over the adjacent coastal ocean, leading to diminished latent heat flux and increased sea-surface temperature (SST). The enhanced SST supports greater atmospheric water vapor, which is accompanied by anomalous wind, and transported into the East China monsoon region.

The increase in atmospheric water vapor favors more cloud cover and precipitation, especially in the eastern afforestation region. Furthermore, the increase in atmospheric water vapor and cloud cover produce a greenhouse effect, raising the wintertime surface air temperature. By comparing simulations in which ocean temperature are either fixed or variable, we demonstrate that a significant hydrologic response in East China to afforestation only occurs if ocean temperatures are allowed to vary and the oceanic source of moisture to the continent is enhanced.

Keywords Afforestation · CCSM3.5 · CLM-DGVM · East China monsoon region · Ocean variability · WES feedback

D. Ma
Key Laboratory for Land Surface Process and Climate Change
in Cold and Arid Regions, Cold and Arid Regions
Environmental and Engineering Research Institute,
Chinese Academy of Science, Lanzhou, China

D. Ma (✉) · M. Notaro · G. Chen
Nelson Institute for Environmental Studies,
Center for Climatic Research, University of Wisconsin-Madison,
1225 West Dayton St., Madison, WI 53706, USA
e-mail: madi@lzb.ac.cn

D. Ma
Graduate School of Chinese Academy of Sciences,
Chinese Academy of Science, Beijing, China

Z. Liu
Laboratory for Climate, Ocean and Atmosphere Studies,
Perking University, Beijing 100871, China

Y. Liu
Center for Forest Disturbance Science,
USDA Forest Service, Athens, GA, USA

1 Introduction

Afforestation has been proposed as a strategy by the Kyoto Protocol for mitigating anthropogenic global warming through carbon sequestration. The Global Forest Resources Assessment (2005) found that China's afforestation and reforestation activities have, to an extent, offset the negative impacts of deforestation in the world (FAO 2005). China plans to increase its percentage forest cover from 18.2 % at present to 26 % by the year 2050 (Lei 2005). In an effort to increase its carbon sink (Yang et al. 2010).

Such an extensive land cover change in China is likely to impact the climate on a variety of spatial scales through direct and indirect interactions within the earth's land/ocean/atmosphere system. Few studies have examined the climatic effect of extreme land cover change in China (Xue 1996; Liu et al. 2008). Liu et al. (2008) used a regional climate model (RCM) to simulate the impact of afforestation in northern China. They found that afforestation

increased precipitation, relative humidity, and soil moisture and reduced wind speed and air temperature, with the greatest effects in spring-summer.

Land cover changes at different latitudes can induce unique climate effects. Tropical deforestation can exacerbate local warming through decreased evaporation and precipitation (Henderson-Sellers et al. 1993; Werth and Avissar 2002). Expansion of the boreal forests can produce warming, mainly through vegetation/snow albedo feedbacks (Bonan et al. 1992; Foley 1994; Betts 2000; Gallimore et al. 2005; Notaro and Liu 2008). In contrast, the climatic impact of changes in temperate forests (e.g. China) is highly uncertain and less understood than that of the tropical and boreal regions (Bonan 2008; Chen et al. 2012). It is unclear whether temperate forest regions like China behaves more like tropical or boreal forests in terms of their climate feedbacks, with the former supporting a moisture feedback and the latter supporting a thermal feedback. Furthermore, its feedback could vary by season.

Numerous studies have isolated mechanisms by which changes in vegetation can affect regional and global climate (Bonan et al. 1992, 2008; Meehl 1994; Xue 1996; Xue et al. 2004; Pielke et al. 1998). Biosphere–atmosphere interactions are often complex and nonlinear, which poses challenges for terrestrial ecosystem models within coupled general circulation models (Bonan 2008). The sign and strength of vegetation feedbacks to the atmosphere depend on the geographical region and background climatology (Notaro et al. 2011a). Changes in vegetation can affect the surface radiation budget, hydrologic cycle, and atmospheric circulation across a range of temporal and spatial scales. A number of mechanisms have been proposed to explain how changes in vegetation cover might affect climate. The vegetation albedo feedback mechanism (e.g. grass versus bare ground) suggests that increased vegetation cover decreases the surface albedo, increases the absorbed solar radiation at the surface, and increases surface temperature (Charney 1975). The snow/vegetation albedo feedback, by which the albedo of forested land with snow is lower than snow-covered soil, can induce a warming in spring (Gallimore and Kutzbach 1996). The evapotranspiration mechanism indicates that increased vegetation cover results in enhanced plant transpiration, resulting in a decrease in surface temperature, increase in water vapor availability and greater precipitation through local moisture recycling (Shukla and Mintz 1982). The roughness length mechanism suggests that increased vegetation height and leaf area index (LAI) (e.g. more trees relative to grass) produces greater surface roughness and decreased wind speed, leading to increased mass convergence into surface low-pressure centers. This, in turn, can induce upward moisture transport and increased convective cloud cover and precipitation. Roughness length changes

also alter the aerodynamic resistance, which affects turbulent fluxes (e.g. latent heat flux) and precipitation (Sud et al. 1988; Chen et al. 2012).

The land, atmosphere and ocean are strongly coupled in the Asian Monsoon system (Yasunari 2007), suggesting that oceans may play a stronger role in modulating vegetation–climate interactions than in regions without a seasonal monsoon. A number of studies have investigated land cover change effects in global climate models (GCMs) with fixed sea surface temperatures (SSTs) (Xue 1996; Kanae et al. 2001; Werth and Avissar 2002; Xue et al. 2004; Sen et al. 2004). For example, Xue et al. (2004) found that both surface albedo and vegetation perturbations are important to the East Asian and West African monsoon evolution and intensity, as well as the spatial distribution of precipitation and atmosphere circulation. In a desertification experiment for the Sahel, Xue and Shukla (1996) found that a reduction in evaporation dominated the response of local surface energy budget.

Studies have also applied fully coupled atmosphere–ocean–land models with dynamic vegetation to examine vegetation feedbacks on climate (Levis et al. 2004; Gallimore et al. 2005; Notaro and Gutzler 2011; Notaro et al. 2011a, b). The study by Notaro et al. (2011a) used a fully coupled atmosphere–ocean–land model to assess vegetation feedbacks on climate for six monsoon regions, including the East China monsoon region, and found that the model captured the major structure of global and regional climatology. In their study, decreased vegetation cover in East China produced year-around warming, increased springtime precipitation, and decreased precipitation in the other seasons. However, these studies did not isolate the modulating effect of the ocean on land–atmosphere interactions. Dallmeyer et al. (2010) studied the impact of oceanic and vegetation feedbacks on Holocene climate change and found that the ocean can modify the atmospheric signal. However, the modulating effect of the ocean on land–atmosphere interactions may differ significantly by region.

This study uses a fully coupled climate model to examine the equilibrium, long-term impacts of afforestation on climate in the East China monsoon region and to explore the potential modulating effect of ocean temperature variability on these afforestation feedbacks to climate. This study differs from previous studies by focusing on the climatic effects of afforestation in a previously deforested temperate region and comparing fixed ocean simulations with fully coupled experiments, in order to isolate the influence of ocean–atmosphere interaction on the climatic response to afforestation in the East China monsoon region.

This study addresses two key questions: (1) what is the long-term effect of afforestation on climate in the East China monsoon region? (2) what role does SST variability

play in modulating afforestation feedbacks on climate? In this paper, the model and experimental design are described in Sect. 2. “Results” of the modeling experiments are described in Sect. 3, and the “Discussion and Conclusions” are presented in Sect. 4.

2 Model and experimental design

2.1 Model description

The model used in this study is the National Center for Atmospheric Research Community Climate System Model Version 3.5 (NCAR CCSM3.5), which includes dynamic atmosphere, land, ocean and sea ice components (Gent et al. 2010). We apply a finite volume dynamical core and a horizontal resolution of $1.9^\circ \times 2.5^\circ$. The land component, the Community Land Model version 3.5 (CLM3.5-DGVM) includes vegetation dynamics with annual vegetation processes based on the Lund-Potsdam-Jena (LPJ) dynamic global vegetation model (Levis et al. 2004). There are ten plant functional types (PFTs) in CLM3.5, including three types of grasses and seven types of trees, and the vegetation performed in CLM3.5-DGVM is potential vegetation. Also, there are 10 soil layers in land model. Several improvements were made to the CLM3.5 version. Compared to previous versions, the partitioning of evapotranspiration (ET) was improved, which resulted in wetter soils, less plant water stress, enhanced transpiration and photosynthesis, and a more reliable annual cycle of total water storage (Oleson et al. 2008). When scaling of the canopy interception was included, a resistance term was added to reduce excessive soil evaporation (Lawrence et al. 2007). The ocean component, the Parallel Ocean Program (POP), uses a dipole grid with a nominal horizontal resolution of 1° . The grid is 1.125° in the zonal direction (320 points) and roughly 0.5° in the meridional direction with higher resolution near the equator. The sea-ice model is integrated on the same horizontal grid as the ocean model (Collins et al. 2006).

2.2 Experimental design

To analyze the long-term influence of afforestation on climate in the fully coupled model, a control run with high tree cover (HIGH_CPL) and a sensitivity run with low tree cover (LOW_CPL) are produced. In HIGH_CPL, the global tree cover can range from 0 to 95 % in each terrestrial grid cell (Table 1). In LOW_CPL, the range in tree cover is the same as in HIGH_CPL, except for in the East China monsoon region (defined as 19.9°N – 41.0°N , 107.5°E – 122.5°E), where it ranges from 0 to a maximum of 65 %. The fully coupled simulations are run for 80 years from the same initial equilibrium state, and the last 70 years are

Table 1 Model design and tree cover range globally and in the East China monsoon region

Simulation	Tree cover range globally (%)	Tree cover range in the East China monsoon region (%)	Ocean	#Years
HIGH_CPL	0–95	0–95	Fully coupled	70
LOW_CPL	0–95	0–65	Fully coupled	70
HIGH_FIX	0–95	0–95	Fixed SST and ice fraction	50
LOW_FIX	0–95	0–65	Fixed SST and ice fraction	50

analyzed. This study is a further exploration of Notaro et al. (2011a). Their earlier study focused on the short-term (1 year) decreased vegetation on climate in six monsoon domains; however, the current study focuses exclusively on the long-term afforestation effect (70 years) in the East China monsoon region.

Moreover, to isolate the role of ocean variability in the afforestation response, we conduct simulations parallel to HIGH_CPL and LOW_CPL, but with prescribed global SSTs and sea ice fraction (Table 1). The SSTs and sea ice fraction are fixed at the global climatology from the 100-year control run (HIGH_CPL). The high tree cover run with prescribed SST is named HIGH_FIX, and the parallel low tree cover sensitivity run is named LOW_FIX. These simulations are 50 years in duration and all years are analyzed. The afforestation produced by HIGH_FIX over LOW_FIX is about the same as for the coupled runs (23 % more tree cover).

In the text, all differences that are described are statistically significant at the $p < 0.1$ level, based on student t -tests, unless stated otherwise.

3 Results

3.1 Vegetation cover change

The major potential vegetation types over the East China monsoon region include temperate broadleaf/needleleaf evergreen forest, evergreen/deciduous mixed forest and grassland/steppe (Ramankutty and Foley 1999). The vegetation types simulated in experiment HIGH_CPL (which include evergreen tree, deciduous tree and grass) are similar to the potential vegetation types identified by Ramankutty and Foley (1999) for East China. The observed vegetation cover over East China is crops and temperate

forests, which is similar to the potential vegetation type over East China.

Comparing the two simulations, the area-averaged total tree (grass) cover in LOW_CPL is 25 % lower (higher) than in HIGH_CPL across the East China monsoon area. The total vegetation cover does not change. The difference in climate between HIGH_CPL and LOW_CPL is attributed to afforestation in the East China monsoon region. The total leaf area index (LAI) increases year round in HIGH_CPL compared to LOW_CPL (Table 2), on average by 1.43 m²/m².

3.2 Impact of afforestation in the fully coupled experiments

3.2.1 Response of temperature and precipitation

In summer, afforestation over East China leads to local cooling by −0.20 °C (Table 2; Fig. 2a), while the surface air

temperature increases by 0.20 °C in Mongolia, northern China, and southern Russia (Fig. 2a). The response in wintertime surface air temperature to afforestation occurs both locally in the afforested region and over the adjacent ocean, including the South China Sea and Bay of Bengal (Fig. 2b). Across the East China monsoon region, the surface air temperature increases by 0.29 °C in winter.

In response to afforestation, precipitation significantly increases annually (0.20 mm/day). Specifically, precipitation increases in summer and winter by 0.31 and 0.21 mm/day, respectively (Table 2). In summer, rainfall is enhanced locally, over the afforested region (Fig. 2c). However, precipitation increases not only around afforested region but also over the adjacent ocean area in winter (Fig. 2d). The area of increased wintertime precipitation over the ocean corresponds to an area of increased SST, hinting at a mechanism by which ocean warming enhances evaporation and atmospheric moisture content, leading to more rainfall.

Table 2 Effects of afforestation in the fully coupled model

Variable	Units	ANN	MAM	JJA	SON	DJF
Total leaf area index	m ² /m ²	1.43	1.43	1.72	1.63	0.96
Surface stress	kg/m/s ²	0.02	0.02	0.03	0.05	0.05
Surface albedo	Fraction	−0.023	−0.023	−0.020	−0.024	−0.029
Surface net shortwave radiation flux	W/m ²	0.92	1.56	0.67	1.66	−0.23
Downward shortwave radiation flux	W/m ²	−7.32	−6.62	−8.53	−4.78	−9.33
Upward shortwave radiation flux	W/m ²	−9.15	−9.73	−9.87	−8.09	−8.88
Surface net longwave radiation flux	W/m ²	2.20	1.80	2.30	1.83	2.86
Downward longwave radiation flux	W/m ²	2.06	1.59	0.72	1.60	4.34
Upward longwave radiation flux	W/m ²	−0.13	−0.21	−1.59	−0.23	1.49
Heat flux into soil layers	W/m ²	−0.03	−0.72	−0.32	0.57	0.34
Total sensible heat fluxes	W/m ²	0.25	1.10	−0.84	0.19	0.56
Sensible heat flux from ground	W/m ²	−2.57	−2.67	−2.06	−2.51	−3.04
Sensible heat flux from vegetation	W/m ²	2.82	3.77	1.21	2.70	3.60
Total latent heat fluxes	W/m ²	2.90	2.98	4.14	2.74	1.73
Latent heat from transpiration	W/m ²	4.60	4.83	7.97	4.30	1.28
Latent heat from canopy evaporation	W/m ²	2.59	2.51	3.95	2.34	1.55
Latent heat from ground evaporation	W/m ²	−4.29	−4.36	−7.78	−3.90	−1.10
Ground temperature	°C	−0.66	−0.87	−1.21	−0.52	−0.05
Surface air temperature	°C	0.05	0.06	−0.16	−0.01	0.29
Precipitation	mm/day	0.20	0.12	0.31	0.15	0.21
Precipitable water	kg/m ²	0.70	0.58	0.58	0.75	0.89
Precipitation minus evaporation	mm/day	0.10	0.01	0.17	0.05	0.15
Total evapotranspiration	mm/day	0.10	0.10	0.14	0.09	0.06
Total cloud cover fraction	Fraction	0.013	0.003	0.011	0.011	0.024
High cloud cover fraction	Fraction	0.010	0.002	0.011	0.013	0.011
Mid-level cloud cover fraction	Fraction	0.008	0.003	0.005	0.009	0.015
Low cloud cover fraction	Fraction	0.010	0.004	0.012	0.002	0.020

Annual and seasonal differences (HIGH_CPL−LOW_CPL) for variables, averaged over the East China monsoon region, with bold values indicating statistically significant differences at $p < 0.1$. ANN, MAM, JJA, SON, and DJF are annual, March–April–May, June–July–August, September–October–November and December–January–February, respectively

3.2.2 Mechanisms governing climatic response to afforestation

In this section, we explore the key processes governing the climatic response to afforestation in the East China monsoon region. First, we examine the components of the surface energy budget across the afforested region (Fig. 1; Table 2). Note that all radiation fluxes directed toward (away from) the surface are defined as positive (negative), while non-radiation fluxes (such as latent heat flux and sensible heat flux) directed toward the surface are defined as negative. The total latent heat flux is comprised of three terms: transpiration, ground evaporation and canopy evaporation. The total sensible heat flux is the sum of the sensible heat fluxes from both the ground and vegetation.

During summer (JJA), in response to the increased tree cover in the East China monsoon region, the surface loses energy through an increase in latent heat flux and gains energy through increases in net longwave and shortwave radiation. The largest change response in the surface energy budget to afforestation is an increase in the total latent heat flux by 4.14 W/m^2 (Table 2; Fig. 1d), which results from several factors. With greater LAI, in HIGH_CPL, plant transpiration and canopy evaporation increase by 7.97 W/m^2 and 3.95 W/m^2 (Table 2), respectively. Meanwhile, with more leaf cover shading the land, ground evaporation decreases by 7.78 W/m^2 . Compared to the latent heat flux, the change in total sensible heat flux is small (-0.84 W/m^2).

Meanwhile, owing to the increase in evapotranspiration, atmospheric moisture and cloud cover in summer generally also increase, which decreases (increases) the downward component of the shortwave (longwave) radiation flux to the surface during summer. Net longwave radiation increases by 2.30 W/m^2 (Table 2; Fig. 1b) due to the combined effects of a decrease in upward longwave radiation flux, in response to surface cooling (1.59 W/m^2), and an increase in the downward longwave radiation flux (0.72 W/m^2). The surface albedo decreases by 0.02 with afforestation due to the lower reflectivity of tree relative to grass, leading to a decrease in the upward reflected component of shortwave radiation. However, the increase in net shortwave radiation flux is not statistically significant.

From the above details, it is shown for summer that the total latent heat flux is the most sensitive component of the surface energy budget for East China. This indicates that increased evapotranspiration is the dominant mechanism producing cooling over the afforested East China monsoon region in summer. In other words, during summer, the hydrologic/moisture feedback dominates over temperate forest of the East China monsoon region.

In winter (DJF), the largest change in the surface energy budget is an increase in net longwave radiation by 2.86 W/m^2

(Fig. 1b), primarily due to an increase in its downward component by 4.34 W/m^2 (Table 2). Compared to the net longwave radiation change, the change in the total latent heat flux is small, while the total sensible heat flux and net shortwave radiation do not significantly change. Meanwhile, even though the surface albedo decreases by 0.03 with afforestation, the net shortwave radiation change is not statistically significant, which is mainly due to the increased cloud cover and associated reduction of downward shortwave radiation. Therefore, the warming response in winter is associated with an increase in the downward component of the longwave radiation flux. We will next examine the reason for the increase in longwave radiation in the afforestation experiments with ocean variability.

3.2.3 The remote ocean effect and response of atmospheric circulation in winter

A key reason for the wintertime increase in SST across the ocean areas adjacent to the afforested region, including the South China Sea, Indian Ocean and Bay of Bengal, is influence of wind speed on the air-sea energy exchange. Over the tropical Indian Ocean and the South China Sea, the warming can be explained by a wind-evaporation-SST (WES) positive feedback (Xie and Philander 1994). In the fully coupled experiment, the climatological surface wind is northeasterly over the Indian Ocean and the South China Sea in winter (Fig. 3a). In response to afforestation, the surface wind speed decreases over the East China monsoon region in the fully coupled experiment (Fig. 3c). This decrease in wind speed over the local region initiates a modest decline in wind speed near the afforestation region, namely the South China Sea, Indian Ocean and Bay of Bengal. Hence, when ocean variability is included, this initial reduction in surface wind speed induces a decline in evaporation (Fig. 3e). Over these ocean regions, SST increases due to this reduction in evaporation (Fig. 2b). This warming further lowers the atmospheric pressure, thereby enhancing convergence (Fig. 3c), and further weakening the surface wind by producing an anomalously southwesterly wind. The further decline in wind speed leads to reduced latent heat flux (Fig. 3e) and an additional increase in SST, comprising a positive WES feedback in the fully coupled model. This feedback explains the warming of the South China Sea, Indian Ocean and Bay of Bengal, differing from the fixed ocean experiments without ocean variability.

The anomalous southwesterly flow in the afforestation case (Fig. 3c) leads to more water vapor transport into the East China monsoon region from the South China Sea (Fig. 4a). This anomalous moisture flux generates greater cloud cover fraction by 0.024 (Table 2) across the monsoon region. Moreover, the local increase in moisture

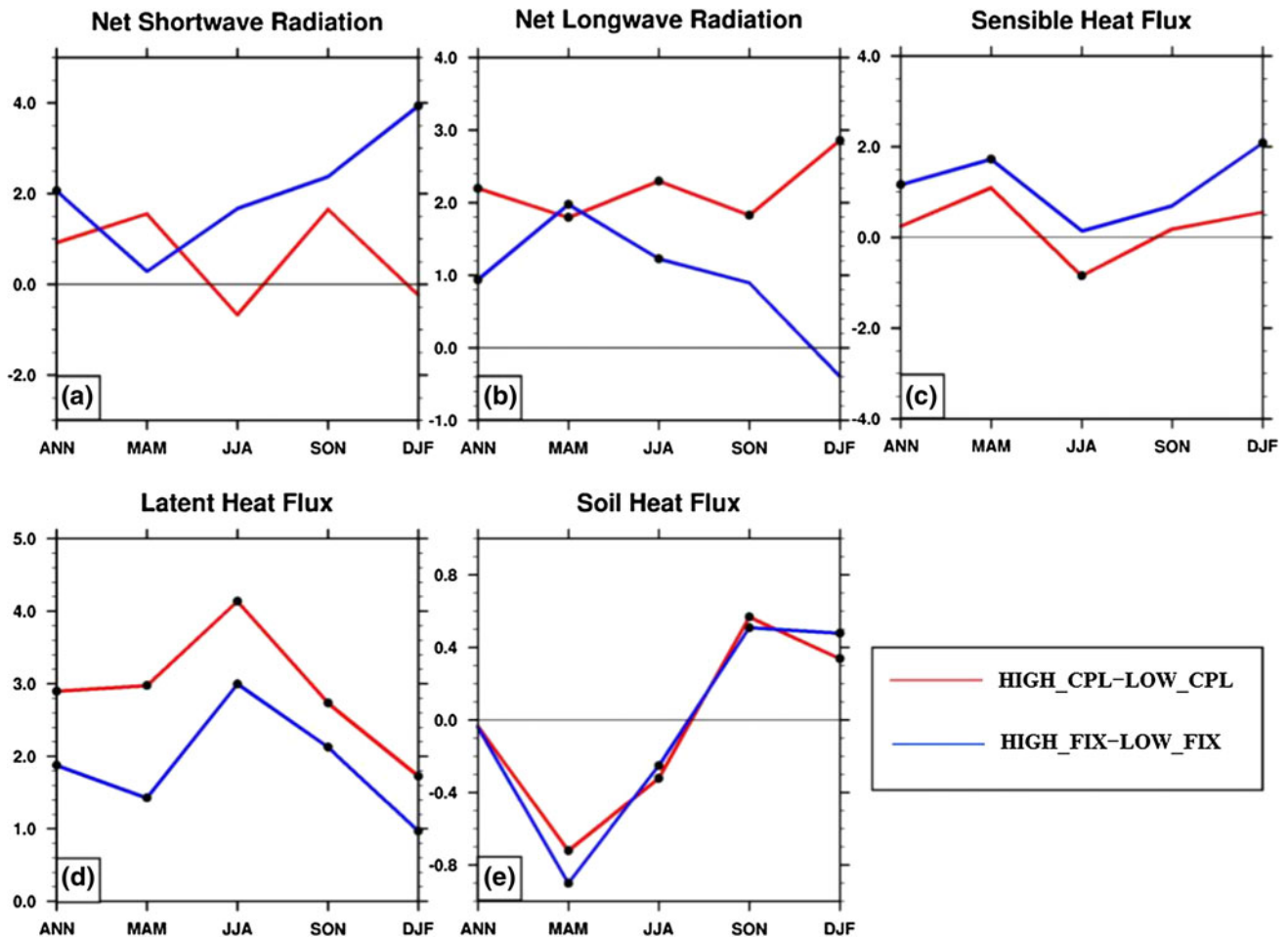


Fig. 1 Differences in surface energy budget components, both seasonally and annually, over the East China monsoon region, including **a** net shortwave radiation, **b** net longwave radiation, **c** total sensible heat fluxes, **d** total latent heat fluxes, and **e** soil heat flux

(W/m^2). Red and blue lines indicate the effects of afforestation in the fully coupled experiments (HIGH_CPL-LOW_CPL) and the fixed ocean experiments (HIGH_FIX-LOW_FIX), respectively. Black dots indicate statistically significant changes ($p < 0.1$)

produces a greenhouse effect, trapping in more longwave radiation and contributing to the warming ($0.23\text{ }^\circ\text{C}$) (Table 2), over the East China monsoon region. Hence, this complex mechanism, which includes the WES positive feedback and greenhouse effect, is the key reason for the winter warming over the East China monsoon region (Fig. 5).

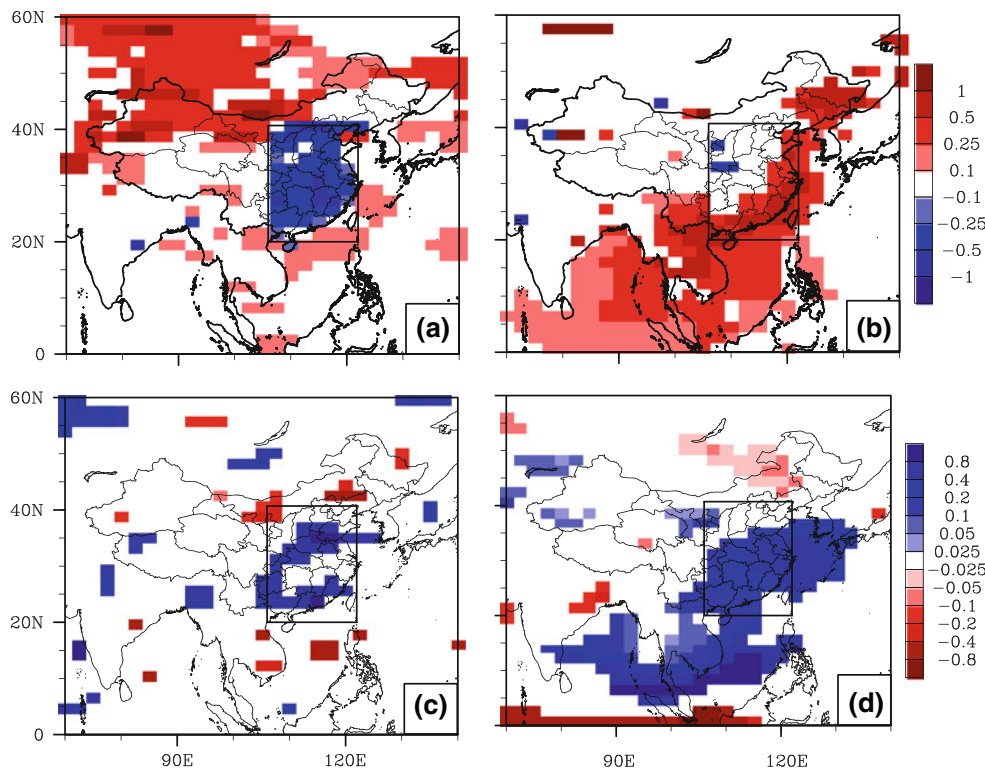
3.3 Impact of afforestation in fixed ocean experiments

The results presented in Sect. 3.2 suggest that remote air-sea interaction plays a vital role in the climatic response to afforestation in the East China monsoon region. In response to afforestation, the surface air temperature significantly increases by $0.25\text{ }^\circ\text{C}$ in winter (Fig. 7a) and decreases by $0.26\text{ }^\circ\text{C}$ in summer in the fixed ocean experiments (Table 3). In summer, the largest change in the surface energy budget is in the total latent heat flux, which increases by $3.00\text{ }W/m^2$. The summer cooling can be

explained by the evapotranspiration (ET) mechanism, as in the fully coupled afforestation experiment.

The warming mechanism in winter in the fixed SST afforestation experiments is different from the fully coupled afforestation experiments (Fig. 6). Comparing the energy budget terms (Fig. 1), in contrast to the coupled runs, the change in net shortwave radiation in the fixed ocean afforestation experiment is larger than all other components of the energy budget. In HIGH_CPL-LOW_CPL, the net shortwave radiation slightly decreases by $-0.23\text{ }W/m^2$; however, it increases significantly by $3.94\text{ }W/m^2$ in HIGH_FIX-LOW_FIX. The increase in net shortwave radiation with afforestation is mainly due to a reduced surface albedo (-0.027), in HIGH_FIX-LOW_FIX. Compared to the fully coupled experiment, the local albedo mechanism dominates the winter air temperature response to afforestation in the fixed ocean afforestation experiments. The resulting surface wind speed changes over the nearby ocean, attributed to afforestation, are smaller in the fixed

Fig. 2 Simulated surface air temperature ($^{\circ}\text{C}$) change due to East China afforestation (HIGH_CPL-LOW_CPL) in **a** JJA and **b** DJF. Simulated precipitation (mm/day) change (HIGH_CPL-LOW_CPL), **c** in JJA **d** in DJF. Color shading is only shown for statistically significant changes ($p < 0.1$). The rectangle indicates the afforested region



ocean experiment (HIGH_CPL-LOW_CPL). This can be explained by the absence of air-sea energy exchange in the fixed ocean runs, which can drive the WES mechanism and induce changes in wind speed in the coupled model.

3.4 Hydrologic response in the two afforestation experiments

The response in the hydrologic cycle in the fully coupled afforestation experiment is greater than in the fixed ocean afforestation experiment. In the East China monsoon region, precipitation does not significantly change in the fixed ocean afforestation experiment (Fig. 8a); however, it significantly increases in the fully coupled afforestation experiment during both summer and winter (Fig. 8a). In the fully coupled afforestation experiment, precipitation increases annually by 0.20 mm/day, with the greatest increase of 0.31 mm/day in summer. During winter, the precipitation increases by 0.21 mm/day (Table 2). In the fixed ocean afforestation experiment, precipitation does not significantly change. Just slightly increases by 0.01 mm/day in summer and winter (Table 3).

The change in annual precipitable water in the fully coupled afforestation experiment is also larger than that in the fixed ocean afforestation experiment. In the fully coupled afforestation experiment, precipitable water across East China increases during winter, pre-monsoon, and monsoon onset (Fig. 8b). Compared to the fully coupled

afforestation experiment, the year-round response in precipitable water is much weaker in the fixed ocean afforestation experiment (Fig. 8b).

The anomalous vertical motion profile differs between the fully coupled afforestation experiment and fixed ocean afforestation experiment. During winter, there is anomalous ascent from 1,000 hPa to 200 hPa in the fully coupled runs over the East China monsoon region (Fig. 9a). This anomalous ascent, combined with more precipitable water, supports greater cloud formation and enhanced precipitation in winter. In contrast, there is no significant change in vertical motion in the fixed ocean experiment during winter (Fig. 9b). Thus, in the fully coupled afforestation experiment, the added water vapor, which is anomalously transported into the East China monsoon region, helps support ascent and latent heat release in the afforested region.

Moreover, in the fully coupled experiment, PME (precipitation minus evapotranspiration) increases 0.17 and 0.06 mm/day in summer and winter, respectively (Table 2). The increase in ET accounts for 45 and 29 % of the increase in total precipitation in summer and winter, respectively (Table 2). It indicates that water vapor from remote region is the key reason for the increased winter precipitation over East China monsoon region. In summer, the increase in LAI with afforestation induces more evapotranspiration and additional water vapor is supplied from remote regions, both of which lead to greater precipitation.

Fig. 3 Simulated climatological surface wind vectors (m/s) in DJF: **a** HIGH_CPL and **b** HIGH_FIX. Simulated differences in surface wind vectors and wind speed in DJF: **c** HIGH_CPL-LOW_CPL and **d** HIGH_FIX-LOW_FIX. Simulated difference in latent heat flux (W m^{-2}) in DJF: **e** HIGH_CPL-LOW_CPL and **f** HIGH_FIX-LOW_FIX. Color shading is shown for statistically significant changes in wind speed and latent heat flux ($p < 0.1$)

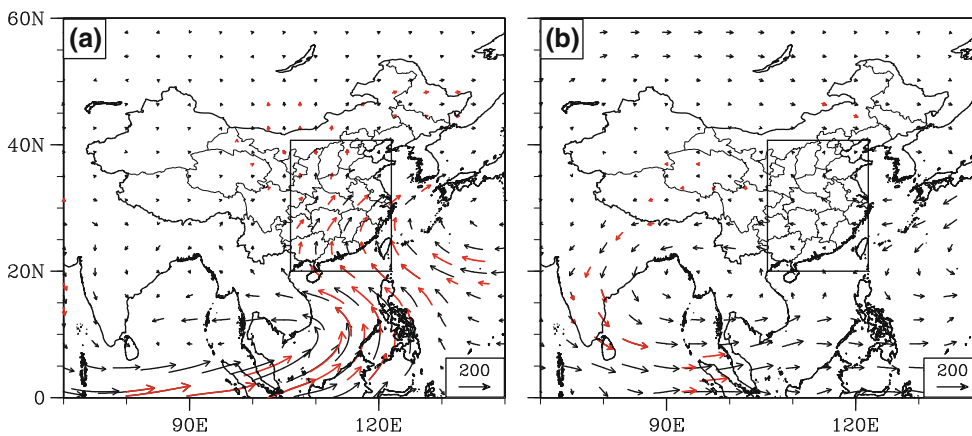
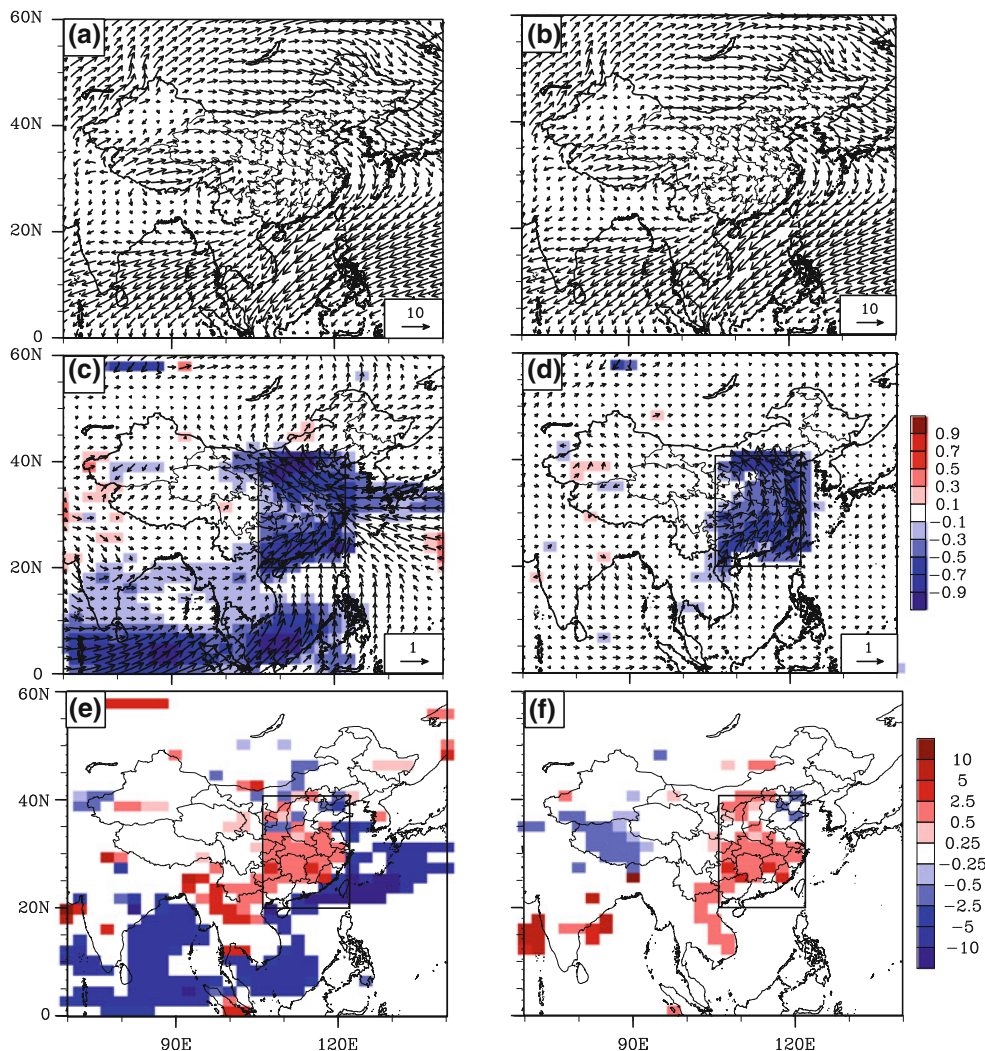


Fig. 4 Simulated differences in column-integrated (from sea surface to 100 hPa) atmospheric water vapor transport vectors (kg/m/s) in DJF: **a** HIGH_CPL-LOW_CPL and **b** HIGH_FIX-LOW_FIX. Red vectors indicate statistically significant changes ($p < 0.1$)

In summary, we find that, in response to afforestation, the local hydrologic cycle is amplified, especially in winter, in the fully coupled experiment. The enhancement of the

hydrologic cycle in the afforested region is in response to more water vapor transport into the East China monsoon region when ocean variability is included (Fig. 4a, b).

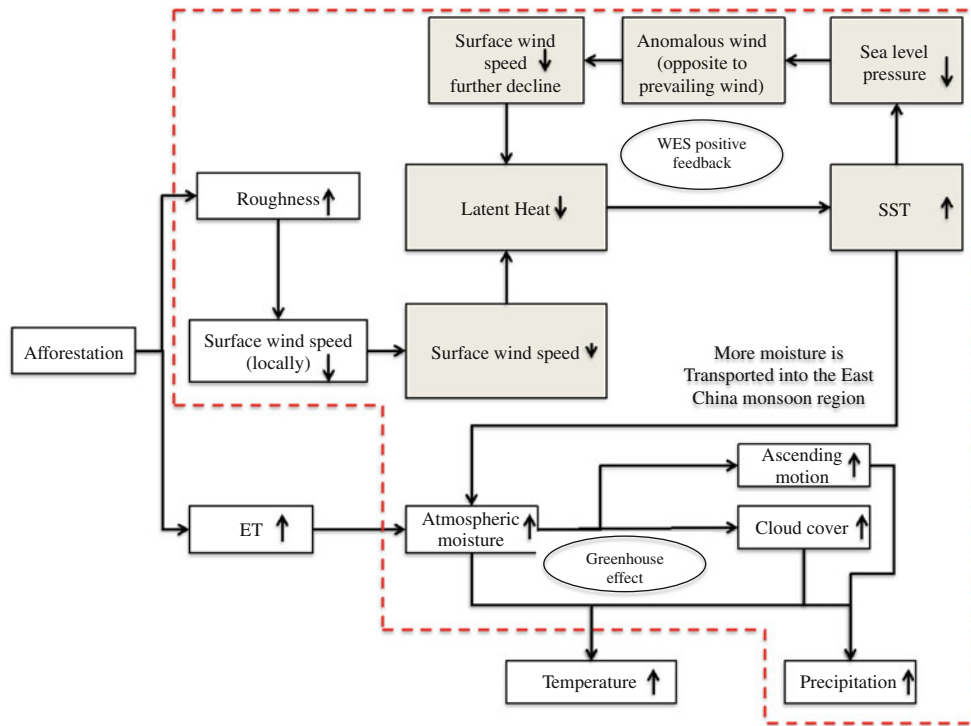


Fig. 5 Schematic diagram of afforestation feedbacks over East China and the nearby ocean during winter with ocean variability included. *Shading* indicates changes over the South China Sea, Bay of Bengal

and part of Indian Ocean. The *red shade line* indicates the dominant mechanism for the change in hydrology

Fig. 6 Schematic diagram of afforestation feedbacks over East China and the nearby ocean during winter without ocean variability included. *Shading* indicates changes over the South China Sea, Bay of Bengal and part of Indian Ocean. *Red rectangles* indicate that significant changes, while *blue rectangles* indicate insignificant changes

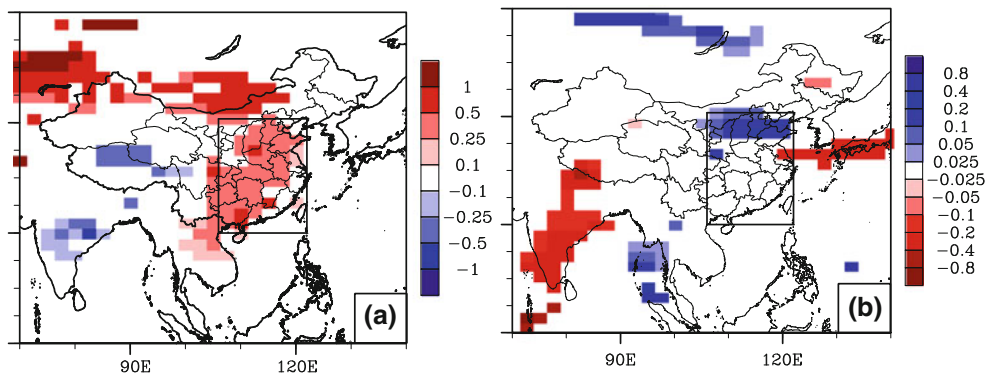
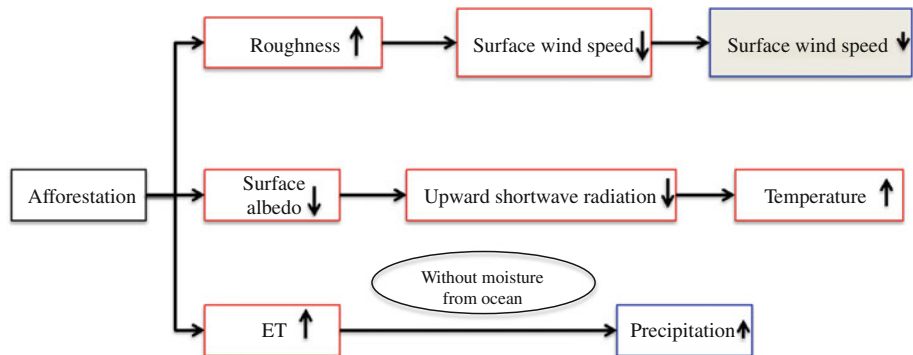


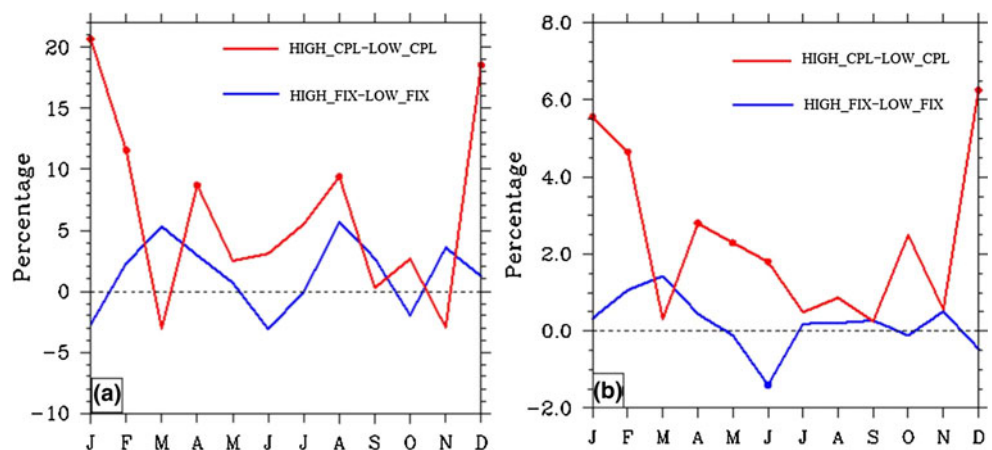
Fig. 7 Change (HIGH_FIX-LOW_FIX) during winter in **a** surface air temperature (°C) and **b** precipitation (mm/day). *Color shading* is only shown for statistically significant changes ($p < 0.1$)

Table 3 Effects of afforestation in the fixed ocean simulations

Variable	Units	ANN	MAM	JJA	SON	DJF
Total leaf area index	m ² /m ²	1.29	1.31	1.62	1.53	0.72
Surface stress	kg/m/s ²	0.02	0.02	0.02	0.03	0.04
Surface albedo	fraction	-0.021	-0.021	-0.018	-0.022	-0.027
Surface net shortwave radiation flux	W/m ²	2.07	0.29	1.68	2.38	3.94
Downward shortwave radiation flux	W/m ²	-1.99	-4.46	-2.63	-1.14	0.29
Upward shortwave radiation flux	W/m ²	-4.06	-4.75	-4.31	-3.52	-3.65
Surface net longwave radiation flux	W/m ²	0.94	1.98	1.23	0.96	-0.39
Downward longwave radiation flux	W/m ²	0.18	0.27	-0.86	-0.16	1.45
Upward longwave radiation flux	W/m ²	-0.76	-1.70	-2.83	-1.12	1.84
Heat flux into soil layers	W/m ²	-0.04	-0.90	-0.25	0.51	0.48
Total sensible heat fluxes	W/m ²	1.17	1.73	0.15	0.70	2.09
Sensible heat flux from ground	W/m ²	-2.07	-2.14	-1.40	-2.00	-2.73
Sensible heat flux from vegetation	W/m ²	3.24	3.87	1.55	2.71	4.83
Total latent heat fluxes	W/m ²	1.88	1.43	3.00	2.13	0.97
Latent heat from transpiration	W/m ²	3.84	3.18	7.06	3.80	1.32
Latent heat from canopy evaporation	W/m ²	1.70	2.28	2.55	1.43	0.54
Latent heat from ground evaporation	W/m ²	-3.66	-4.04	-6.61	-3.10	-0.90
Ground temperature	°C	-0.65	-1.01	-1.14	-0.56	0.12
Surface air temperature	°C	-0.12	-0.26	-0.29	-0.20	0.25
Precipitation	mm/day	0.05	0.10	0.01	0.07	0.01
Precipitable water	kg/m ²	0.03	0.13	-0.14	0.06	0.05
Precipitation minus evaporation	mm/day	-0.02	0.05	-0.07	-0.03	-0.03
Total evapotranspiration	mm/day	0.06	0.05	0.10	0.07	0.03
Total cloud cover fraction	Fraction	0.004	0.01	0.006	0.004	-0.004
High cloud cover fraction	Fraction	0.003	0.006	0.004	0.004	-0.004
Mid-level cloud cover fraction	Fraction	0.002	0.006	-0.001	0.002	0.001
Low cloud cover fraction	Fraction	0.005	0.01	0.01	0.004	-0.004

Same as Table 2, except HIGH_FIX-LOW_FIX

Fig. 8 Simulated percent differences in **a** precipitation and **b** precipitable water, across the East China monsoon region. From the fully coupled afforestation experiments (HIGH_CPL-LOW_CPL) (red) and the fixed ocean afforestation experiments (HIGH_FIX-LOW_FIX) (blue), respectively. Dots indicate statistically significant changes ($p < 0.1$)



4 Discussion and conclusions

In order to study the potential impacts of afforestation on climate in the East China monsoon region, and to

furthermore investigate the role of ocean variability in modulating the climatic response to afforestation, two sets of experiments are conducted: fully coupled afforestation simulations and fixed ocean afforestation simulations.

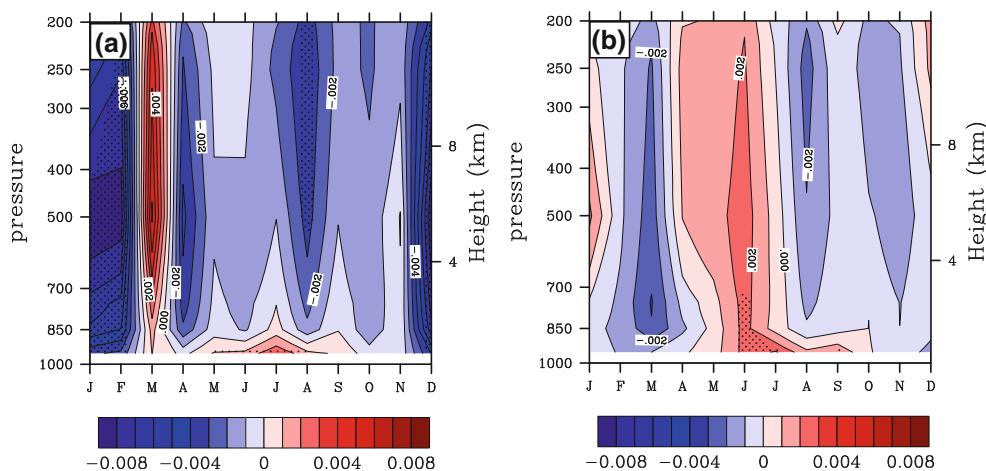


Fig. 9 Simulated differences in the vertical profiles of vertical motion (Pa/s) in the **a** fully coupled simulations (HIGH_CPL-LOW_CPL) and the **b** fixed SST simulations (HIGH_FIX-LOW_FIX). *Black dots* indicate statistically significant changes ($p < 0.1$)

During summer, afforestation over East China in the fully coupled model results in a cooler climate in response to increased evapotranspiration, which is consistent with the study by Dallmeyer and Clauseen (2011). Swann et al. (2012) found that afforestation over the mid-latitudes may lead to annually warming due to soil water limitation. The main reason that our study differs from that of Swann et al. (2012) is that the East China monsoon region is close to the Tropics, so plants and soil can access enough water for evapotranspiration.

During winter, the mechanism for warming differs between experiments in which ocean variability is either included or excluded. With ocean variability, the warming effect is mainly caused by the local increase in roughness length and its influence on the wind field. In response to afforestation, the denser forest induces higher surface stress, which triggers a nearby increase in SSTs due to the inclusion of the WES feedback. In turn, the increase in nearby SSTs leads to warmer air and produces low air pressure overlying the ocean. Hence, the moister and warmer air can transport inland from South China Sea. The enhanced water vapor can form clouds and trapping more longwave radiation, thereby warming the atmosphere in eastern China. Therefore, the ocean plays an important role in modulating vegetation feedbacks to climate.

During winter, by fixing SSTs, there is no WES feedback included, since wind speed cannot influence on SSTs. The initial modest decline in surface wind speed cannot induce an increase in SST and further weak surface wind speed over the South China Sea and Bay of Bengal. Different from the fully coupled afforestation experiments, the warming over the East China monsoon region in the fixed SST experiments is mainly caused by a local decrease in surface albedo and an associated increase in absorbed solar radiation. This mechanism is consistent with the study of Dallmeyer and Clauseen (2011).

By including ocean variability, the hydrologic cycle is accelerated over East China in the afforestation simulation. Precipitation and precipitable water significantly increase annually and in winter. More remote atmospheric water vapor is transported inland, leading to the development of greater cloud cover and precipitation. However, the precipitation and precipitable water do not significantly change in the fixed ocean afforestation experiment. The hydrologic cycle is therefore amplified by ocean dynamics, and vegetation feedbacks can only influence the regional hydrology when ocean temperatures are allowed to vary.

In summary, afforestation over the temperate forest regions of the East China monsoon region produces a significant moisture feedback during summer, similar to that of tropical forests. During winter, the climate feedback of afforestation over this temperate forest region is complex, and depends on ocean variability.

It should be noted that the model used in this study has several limitations. It produces excessive LAI, which could generate excessive transpiration and amplify the hydrology cycle (Notaro et al. 2011a). The model is capable of simulating the monsoons seasonal cycle but the monsoons are too wet and penetrate too far inland (Notaro et al. 2011a). Also, the afforestation experiment designed here is an extensive land cover change, which is likely not realistic.

The work presented here suggests that when imposing land cover changes in climate models, ocean variability should be included. With or without ocean temperature variability, the results and responsible mechanisms can be totally different.

Acknowledgments The USDA Forest Service, NSF, 2012CB955200, GYHY200906016, 2010CB950503 and China Scholarship Council funded this work. The simulations were made using NERSC computer resources. The authors thank Dr. Robert Gallimore, Bjorn Brooks, Fuyao Wang and Xinyao Rong for discussion.

References

- Betts RA (2000) Offset of the potential carbon sink from boreal forestation by decreases in surface albedo. *Nature* 408:187–190
- Bonan GB (2008) Forests and climate change: forcings, feedbacks, and the climate benefits of forests. *Science* 320:1444–1449
- Bonan GB, Pollard D, Thompson SL (1992) Effects of boreal forest vegetation on global climate. *Nature* 359:716–718
- Charney JG (1975) Dynamics of deserts and drought in the Sahel. *Q J R Meteor Soc* 101:193–202
- Chen G, Notaro M, Liu Z, Liu Y (2012) Simulated local and remote biophysical effects of afforestation over Southeast United States in boreal summer. *J Clim* (in press). doi:10.1175/JCLI-D-11-00317.1
- Collins WD et al (2006) The community climate system model version 3 (CCSM3). *J Clim* 19:2122–2143. doi:10.1175/JCLI3761.1
- Dallmeyer A, Clauseen M (2011) The influence of land cover change in the Asian monsoon region on present-day and mid-Holocene climate. *Biogeosciences* 8:1499–1519
- Dallmeyer A, Claussen M, Otto J (2010) Contribution of oceanic and vegetation feedbacks to Holocene climate change in monsoonal Asia. *Clim Past* 6:195–218. doi:10.5194/cp-6-195-2010
- FAO (2005) Global forest resources assessment 2005. Rome
- Foley JA (1994) The sensitivity of the terrestrial biosphere to climate-change—a simulation of the middle Holocene. *Global Biogeochem Cycles* 8:505–525
- Gallimore RG, Kutzbach JE (1996) Role of orbitally induced changes in tundra area in the onset of glaciation. *Nature* 381:503–505
- Gallimore R, Jacob R, Kutzbach J (2005) Coupled atmosphere-ocean-vegetation simulations for modern and mid-Holocene climates: role of extratropical vegetation cover feedbacks. *Clim Dyn* 25:755–776
- Gent PR, Yeager SG, Neale RB, Levis S, Bailey DA (2010) Improvements in a half degree atmosphere/land version of the CCSM. *Clim Dyn* 34:819–833. doi:10.1007/s00382-009-0614-8
- Henderson-Sellers A, Dickinson RE, Durbidge TB, Kennedy PJ, Mcguffie K, Pitman AJ (1993) Tropical deforestation: modeling local- to regional-scale climate change. *J Geophys Res* 98(D4):7289–7315. doi:10.1029/92JD02830
- Kanae S, Oki T, Musiak K (2001) Impact of deforestation on regional precipitation over the Indochina peninsula. *J Hydrometeorol* 2:51–70
- Lawrence DM, Thornton PE, Oleson KW, Bonan GB (2007) The partitioning of evapotranspiration into transpiration, soil evaporation, and canopy evaporation in a GCM: impacts on land-atmosphere interaction. *J Hydrometeorol* 8:862–880
- Lei JF (2005) Forest resources of China. China Forestry Publishing House, Beijing
- Levis S, Bonan GB, Bonfils C (2004) Soil feedback drives the mid-Holocene North African monsoon northward in fully coupled CCSM2 simulations with a dynamic vegetation model. *Clim Dyn* 23:791–802
- Liu YQ, Stanturf J, Lu HQ (2008) Modeling the potential of the northern China forest shelterbelt in improving hydroclimate conditions. *J Am Water Res Assoc* 44:1–17. doi:10.1111/j.1752-1688.2008.20240.x
- Meehl GA (1994) Coupled land-ocean-atmosphere processes and South Asian monsoon variability. *Science* 266:263–267
- Notaro M, Gutzler D (2011) Simulated impact of vegetation on climate across the North American monsoon region in CCSM3.5. *Clim Dyn*. doi:10.1007/s00382-010-0990-0
- Notaro M, Liu Z (2008) Statistical and dynamical assessment of vegetation feedbacks on climate over the boreal forests. *Clim Dyn* 31:691–712
- Notaro M, Chen GS, Liu Z (2011a) Vegetation feedbacks to climate in the global monsoon regions. *J Clim*. doi:10.1175/2011JCLI4237.1
- Notaro M, Wyrwoll KH, Chen GS (2011b) Did aboriginal vegetation burning impact on the Australian summer monsoon? *Geophys Res Lett* 38:L11704. doi:10.1029/2011GL047774
- Oleson KW et al (2008) Improvements to the Community Land Model and their impact on the hydrological cycle. *J Geophys Res* 113:G01021. doi:10.1029/2007JG000563
- Pielke RA, Avissar R, Raupach M, Dolman AJ, Zeng X, Denning AS (1998) Interactions between the atmosphere and terrestrial ecosystems: influence on weather and climate. *Global Chang Biol* 4:461–475
- Ramankutty N, Foley J (1999) Estimating historical changes in global land cover: croplands from 1700 to 1992. *Global Biogeochem Cycles* 13:997–1028
- Sen OL, Wang Y, Wang B (2004) Impact of Indochina deforestation on the East-Asian summer monsoon. *J Clim* 17:1366–1380
- Shukla J, Mintz Y (1982) Influence of land-surface evaporation on Earth's climate. *Science* 215:1498–1501
- Sud YC, Shukla J, Mintz Y (1988) Influence of land-surface roughness on atmospheric circulation and precipitation: a sensitivity study with a general circulation model. *J Appl Meteor* 27:1036–1054
- Swann ALS, Fung IY, Chiang JCH (2012) Mid-latitude afforestation shifts general circulation and tropical precipitation. *Proc Natl Acad Sci* 109:712–716
- Werth D, Avissar R (2002) The local and global effects of Amazonian deforestation. *J Geophys Res* 107:8087. doi:10.1029/2001JD000717
- Xie SP, Philander SGH (1994) A coupled ocean-atmosphere model of relevance to the ITCZ in the eastern Pacific. *Tellus A* 46:340–350
- Xue Y (1996) The impact of desertification in the Mongolian and the Inner Mongolian grassland on the regional climate. *J Clim* 9:2173–2189
- Xue Y, Shukla J (1996) The influence of land surface properties on Sahel climate, part II, Afforestation. *J Clim* 9:3260–3275
- Xue Y, Juang HMH, Li WP, Prince S, DeFries R, Jiao Y, Vasic R (2004) Role of land surface processes in monsoon development: East Asia and West Africa. *J Geophys Res* 109:D03105. doi:10.1029/2003JD003556
- Yang XH, Wang XP, Li NY (2010) Combating climate change: what will China's industry do? *R Swed Acad Sci* 39:340–343
- Yasunari T (2007) Role of land atmosphere interaction on Asian monsoon climate. *J Meteorol Soc Jpn* 85:55–75